Articles

Poliovirus RNA-Dependent RNA Polymerase ($3D^{pol}$): Pre-Steady-State Kinetic Analysis of Ribonucleotide Incorporation in the Presence of Mg^{2+} †

Jamie J. Arnold and Craig E. Cameron*

Department of Biochemistry and Molecular Biology, The Pennsylvania State University, University Park, Pennsylvania 16802

Received July 10, 2003; Revised Manuscript Received December 23, 2003

ABSTRACT: We have solved the complete kinetic mechanism for correct nucleotide incorporation catalyzed by the RNA-dependent RNA polymerase from poliovirus, $3D^{pol}$. The phosphoryl-transfer step is flanked by two isomerization steps. The first conformational change may be related to reorientation of the triphosphate moiety of the bound nucleotide, and the second conformational change may be translocation of the enzyme into position for the next round of nucleotide incorporation. The observed rate constant for nucleotide incorporation by $3D^{pol}$ (86 s^{-1}) is dictated by the rate constants for both the first conformational change (300 s^{-1}) and phosphoryl transfer (520 s^{-1}). Changes in the stability of the "activated" ternary complex correlate best with changes in the observed rate constant for incorporation resulting from modification of the nucleotide. With the exception of UTP, the K_d values for nucleotides are at least 10-fold lower than the cellular concentration of the corresponding nucleotide. Our data predict that transition mutations should occur at a frequency of 1/15000, transversion mutations should occur at a frequency of less than 1/150000, and incorporation of a 2′-deoxyribonucleotide with a correct base should occur at a frequency 1/7500. Together, these data support the conclusion that $3D^{pol}$ is actually as faithful as an exonuclease-deficient, replicative DNA polymerase. We discuss the implications of this work on the development of RNA-dependent RNA polymerase inhibitors for use as antiviral agents.

One positive aspect of the human immunodeficiency virus (HIV)[1] pandemic was the realization that, given the appropriate effort, antiviral agents targeting enzymes required for virus multiplication can be developed. The first HIV-encoded enzyme that emerged as a tractable target was the viral polymerase, reverse transcriptase (RT) (*1*−*3*). While most of the inhibitors of HIV RT currently in use are nucleoside analogues (*1*, *4*), many nonnucleoside analogue inhibitors of HIV RT have also been reported (*1*, *4*). In all cases, however, an understanding of the specificity and/or precise mechanism of action of these inhibitors has required evaluation of these compounds in the context of the complete kinetic mechanism for nucleotide incorporation catalyzed by this enzyme (*1*, *4*−*7*) and has benefited from structural information available for HIV RT in the absence and presence of substrates and/or inhibitors (*8*−*14*). Kinetic analysis of site-directed mutants of HIV RT has established some of the fundamental mechanisms employed by this enzyme to recognize its substrates, both nucleic acid and nucleotide, and to cooperate with other viral proteins during the process of converting the viral single-stranded RNA genome into double-stranded DNA (*1*, *4*, *15*, *16*). In addition, mechanistic studies of HIV RT have suggested alternative strategies to target regions of this enzyme distinct from the catalytic center for the design of more specific, less toxic anti-HIV therapeutics (*17*−*22*).

Given the success of the antiviral programs targeting HIV RT, it is quite reasonable to expect that RNA virus polymerases will also prove to be suitable targets for clinical intervention in the treatment of diseases ranging from the common cold to hepatitis. With this goal in mind, we have worked to develop the tools necessary to elucidate the kinetic mechanism for nucleotide incorporation catalyzed by an RNA-dependent RNA polymerase (RdRP) (*23*). As discussed above, elaboration of the complete kinetic mechanism for RdRP-catalyzed nucleotide incorporation will permit elucidation of the structure−function relationships of this class of enzymes, evaluation of inhibitors, and a more direct (i.e., kinetic and thermodynamic) comparison of this enzyme to members of the other classes of nucleic acid polymerases.

† This work was supported, in part, by a Howard Temin Award (CA75118) from the NCI, National Institutes of Health, and by a grant (AI45818) from the NIAID, National Institutes of Health (both to C.E.C.). C.E.C. is the recipient of an Established Investigator Award (0340028N) from the American Heart Association.

* To whom correspondence should be addressed. Tel: 814-863-8705. Fax: 814-865-7927. E-mail: cec9@psu.edu.

[1] Abbreviations: HIV, human immunodeficiency virus; RT, reverse transcriptase; RdRP, RNA-dependent RNA polymerase; ATP, adenosine 5′-triphosphate; 2-APTP, 2-aminopurine 5′-triphosphate; TLC, thin-layer chromatography; NTP, nucleoside 5′-triphosphate; EDTA, ethylenediaminetetraacetic acid; PAGE, polyacrylamide gel electrophoresis; AMP, adenosine 5′-monophosphate; PP_i, pyrophosphate; UTP, uridine 5′-triphosphate; UMP, uridine 5′-monophosphate; 2′-dATP, 2′-deoxyadenosine 5′-triphosphate; 2′-dAMP, 2′-deoxyadenosine 5′-monophosphate; KF, klenow fragment; rNTP, ribonucleoside triphosphate; 2′-dNTP, 2′-deoxynucleoside 5′-triphosphate.

10.1021/bi035212y CCC: $27.50
Published on Web 04/15/2004

Knowledge of the mechanistic differences that exist between the viral RdRP and cellular polymerases should assist in the design of specific inhibitors of the viral enzyme.

The RdRP that we have chosen to study first is the enzyme from poliovirus, $3D^{pol}$. This enzyme can be produced in milligram quantities (*24*), its crystal structure is available (*25*), and we have constructed structural models for its complexes with primer/template and nucleotide (*26*). Moreover, we recently solved the primary problem that has precluded mechanistic studies of $3D^{pol}$, namely, the inability to assemble $3D^{pol}$−primer/template complexes and to monitor enzyme activity by extension of end-labeled primers (*23*). In this report, we describe the complete kinetic mechanism for single nucleotide incorporation catalyzed by poliovirus polymerase in the presence of Mg^{2+}. This study has uncovered several mechanistic differences between the RdRP, RT, and cellular DNA polymerases that can be exploited in developing the RdRP as a target for antiviral therapeutics.

EXPERIMENTAL PROCEDURES

Materials. [γ-^{32}P]ATP (>7000 Ci/mmol) was from ICN; [α-^{32}P]ATP (3000 Ci/mmol), [γ-^{32}P]ATP (3000 Ci/mmol), and [^{32}P]PP_i (6.4 Ci/mmol) were from New England Nuclear; nucleoside 5′-triphosphates, 2′-deoxynucleoside 5′-triphosphates (all nucleotides were ultrapure solutions), and adenosine 5′-*O*-(1-thiotriphosphate) (ATPαS) were from Amersham Pharmacia Biotech, Inc.; 3′-deoxyadenosine 5′-triphosphate (cordycepin) was from Sigma; 2-aminopurine 5′-triphosphate (2-APTP) was generously provided by Larry C. Sowers (Department of Biochemistry and Microbiology, School of Medicine, Loma Linda University, Loma Linda, CA); all RNA oligonucleotides were from Dharmacon Research, Inc. (Boulder, CO); T4 polynucleotide kinase was from New England Biolabs, Inc.; poly(ethylenimine)−cellulose TLC plates were from EM Science; sodium pyrophosphate was from American Bioanalytical; lithium chloride, sodium acetate, and urea were from Fisher; all other reagents were of the highest grade available from Sigma, Fisher, or VWR.

Expression and Purification of $3D^{pol}$. Expression and purification of $3D^{pol}$ were performed as described previously (*24*).

Purification, 5′-^{32}P Labeling, and Annealing of sym/sub. RNA oligonucleotides were purified, labeled, and annealed as described previously (*23*).

$3D^{pol}$ Assays. Reactions contained 50 mM HEPES, pH 7.5, 10 mM 2-mercaptoethanol, 5 mM $MgCl_2$ or $MnCl_2$, 60 μM $ZnCl_2$, nucleotide, sym/sub, and $3D^{pol}$. Reactions were performed at 30 °C. $3D^{pol}$ was diluted immediately prior to use in 50 mM HEPES, pH 7.5, 10 mM 2-mercaptoethanol, 60 μM $ZnCl_2$, and 20% glycerol. Zn^{2+} was added to increase the stability of the enzyme; however, the level of Zn^{2+} employed is insufficient to support nucleotide incorporation. The volume of enzyme added to any reaction was always less than or equal to one-tenth the total volume. Reactions were quenched by addition of EDTA to a final concentration of either 50 mM or 0.3 M or by addition of HCl to a final concentration of 1 M. Immediately after the addition of HCl, the solution was neutralized by addition of 1 M KOH and 300 mM Tris (final concentration). Specific concentrations of primer/template and $3D^{pol}$, along with any deviations from the above, are indicated in the appropriate figure legend.

Rapid Chemical-Quench-Flow Experiments. Rapid mixing/quenching experiments were performed by using a Model RQF-3 chemical-quench-flow apparatus (KinTek Corp., Austin, TX). Experiments were performed at 30 °C by using a circulating water bath. $3D^{pol}$−sym/sub complexes were assembled by mixing $3D^{pol}$ and sym/sub for 3 min at room temperature and then rapidly mixed with the nucleotide substrate. After mixing, reactant concentrations were reduced by 50%. Reactions were quenched either by addition of EDTA to a final concentration of 0.3 M or by addition of HCl to a final concentration of 1 M. Immediately after the addition of HCl, the solution was neutralized by addition of 1 M KOH and 300 mM Tris (final concentration).

Product Analysis: *Denaturing PAGE*. An equal volume of loading buffer (90% formamide, 0.025% bromophenol blue, and 0.025% xylene cyanol) was added to 10 μL of the quenched reaction mixtures and heated to 70 °C for 2−5 min prior to loading 5 μL on a denaturing 23% polyacrylamide gel containing 1× TBE and 7 M urea. Electrophoresis was performed in 1× TBE at 90 W. Gels were visualized by using a phosphorimager and quantified by using the ImageQuant software (Molecular Dynamics).

Data Analysis. Data were fit by nonlinear regression using the program KaleidaGraph (Synergy Software, Reading, PA). Time courses at fixed nucleotide concentration were fit to

$$[\text{product}] = Ae^{-k_{obs}t} + C \quad (1)$$

where A is the amplitude of the burst, k_{obs} is the observed first-order rate constant describing the burst, t is the time, and C is a constant. The apparent binding constant ($K_{d,app}$) and maximal rate constant for nucleotide incorporation (k_{pol}) were determined using the equation:

$$k_{obs} = \frac{k_{pol}[\text{NTP}]}{K_{d,app} + [\text{NTP}]} \quad (2)$$

The pulse−quench data were fit to an equation describing a two-step, irreversible process:

$$[\text{product}] = A\left(1 + \frac{k_2 e^{-k_1 t} - k_1 e^{-k_2 t}}{k_1 - k_2}\right) \quad (3)$$

where A is the amplitude of the burst, k_1 is the rate constant for the first phase, k_2 is the rate constant for the second phase, and t is the time. The value for the equilibrium constant across the conformational-change step was determined using the equations (*27*):

$$k_{chem} = k_{pol}\Lambda_2\frac{\sigma - 1}{E_{obs} - 1} \quad (4)$$

$$K_2 = \frac{1}{\Lambda_2 - 1} \quad (5)$$

$$K_2 = \frac{k_{+2}}{k_{-2}} \quad (6)$$

k_{chem} is the rate constant for the chemical step, k_{pol} is the maximal rate constant for nucleotide incorporation, σ is the

maximal elemental effect, E_{obs} is the observed elemental effect, and k_{+2} and k_{-2} are the forward and reverse rate constants for the conformational-change step, respectively. The true K_d value for ATP dissociating from the 3D^{pol}−sym/sub−ATP complex was determined using

$$K_d = K_{d,app}(1 + K_2) \quad (7)$$

Kinetic Simulation. Kinetic simulations were performed by using KinTekSim Version 2.03 (KinTek Corp., Austin, TX). All rate constants were determined experimentally, except where noted. The agreement between the experimental data and kinetic simulations was determined by visual inspection.

RESULTS

In this paper, we describe a series of experiments that have led to the solution of the complete kinetic mechanism for single nucleotide incorporation catalyzed by the RNA-dependent RNA polymerase from poliovirus, 3D^{pol}. These studies have benefited from the development of a symmetrical primer/template substrate (sym/sub) of defined sequence that permits the evaluation of single and multiple cycles of nucleotide incorporation (*23*). Our combined biochemical and biological studies of 3D^{pol} have demonstrated that 3D^{pol}−sym/sub complexes recapitulate a biologically relevant elongation complex (*26*). Therefore, it is likely that insight gleaned from analysis of the mechanism of nucleotide incorporation in vitro is likely to be relevant to this reaction in vivo. It should be noted that binding of sym/sub to 3D^{pol} is slow; however, this initial 3D^{pol}−sym/sub complex isomerizes into a very stable, catalytically competent complex with a half-life of at least 2 h (*23*). Therefore, in the experiments described herein, neither binding nor dissociation of sym/sub is considered.

Assembly of 3D^{pol}−sym/sub Complexes. In each experiment, unless indicated otherwise, the 3D^{pol}−sym/sub complex was formed by mixing 2 μM 3D^{pol} with 1 μM sym/sub duplex, yielding approximately 0.32 μM complex (see Experimental Procedures for details). This value is in excellent agreement with that predicted by our previously published mechanism for 3D^{pol}−sym/sub complex assembly (*23*). The inability to bind all of the sym/sub in the mixture is due to thermal inactivation of 3D^{pol} during the assembly process (*23*). The amount of complex employed in each reaction is reduced by a factor of 2 relative to that assembled as a result of dilution upon addition of the nucleotide substrate(s).

3D^{pol}-Catalyzed Incorporation of AMP into sym/sub. We first evaluated the dependence of the rate of AMP incorporation into sym/sub on the concentration of ATP. In each experiment, the 3D^{pol}−sym/sub complex was rapidly mixed with ATP (60−600 μM final) and the reaction quenched at various times (5−100 ms) by addition of EDTA (0.3 M final). Product was resolved from substrate by electrophoresis through a denaturing polyacrylamide gel, visualized by phosphorimaging, and quantified by using the ImageQuant software (Molecular Dynamics). Product was plotted as a function of time, and the data (Figure 1A) were fit to a single exponential (eq 1) in order to determine the observed rate constant (k_{obs}) for AMP incorporation into sym/sub at each concentration of ATP employed (data not shown). The observed rate constant for AMP incorporation into sym/sub was plotted as a function of ATP concentration, and the data were fit to a hyperbola (eq 2) which gives an apparent dissociation constant ($K_{d,app}$) of 134 μM for loss of ATP from the 3D^{pol}−sym/sub−ATP complex and a maximal rate constant of 87 s^{-1} for AMP incorporation into sym/sub (Figure 1B, Table 1). The ability to fit the data to a hyperbola was consistent with the minimal mechanism for nucleotide incorporation shown in Scheme 1. Similar observations have been made for all polymerases that have been evaluated in this manner (*5*, *27*−*30*).

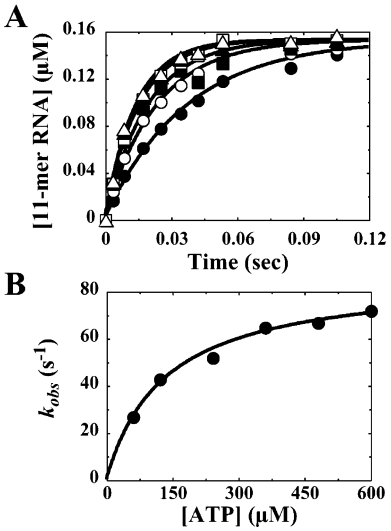

FIGURE 1: Determination of $K_{d,app}$ and k_{pol} for AMP incorporation into sym/sub. (A) 2 μM 3D^{pol} was incubated with 2 μM sym/sub (1 μM duplex) and rapidly mixed with either 60, 120, 240, 360, 480, or 600 μM ATP (final concentrations) as described under Experimental Procedures. The solid lines represent the kinetic simulation of the mechanism shown in Scheme 2 with the kinetic parameters shown in Table 2 for AMP incorporation into sym/sub by 3D^{pol} at ATP concentrations (final) of 60 (●), 120 (○), 240 (■), 360 (□), 480 (▲), or 600 (△) μM. (B) k_{obs} as a function of ATP concentration obtained from the reactions described in (A). The solid line represents the fit of the data to a hyperbola with a $K_{d,app}$ for ATP of 134 ± 18 μM and a k_{pol} of 86.7 ± 3.7 s^{-1}.

Rate-Limiting Steps for Incorporation of AMP into sym/sub. With the DNA polymerases and reverse transcriptases, the rate-limiting step for nucleotide incorporation is a conformational change of the polymerase−primer/template−nucleotide complex (*27*, *28*, *31*). Evidence for a rate-limiting, conformational-change step can be obtained by determining whether a nucleotide substrate containing a phosphorothioate at the α position gives rise to a change in the observed rate constant for nucleotide incorporation. For this experiment, we employed a pure solution of the S_p isomer of ATPαS. Comparison of the kinetics of AMP incorporation into sym/sub to that of AMPαS incorporation showed an elemental effect of 3.8 (Figure 2). Evaluation of the concentration dependence of AMPαS incorporation into sym/sub showed that the reduction in the observed incorporation rate was not due to a change in the apparent dissociation constant for ATPαS relative to ATP (Table 1) and revealed that the maximal elemental effect was 4.2.

If phosphoryl transfer is the rate-limiting step, then an elemental effect between 4 and 11 should be observed (*32*). Because the value of 4.2 determined above is so close to the lower end of the theoretical limit, it was necessary to

Table 1: Kinetic Constants for 3D^{pol}-Catalyzed Nucleotide Incorporation[a]

substrate		kinetic parameter	
nucleic acid	nucleotide	$K_{d,app}$ (μM)	k_{pol} (s^{-1})
sym/sub-U			
GCA**U**GGGCCC	ATP	134 ± 18	86.7 ± 3.7
CCCGGG**U**ACG	ATPαS	89 ± 24	20.6 ± 1.6
	ATP[b]	7.8 ± 1.0	0.83 ± 0.01
	ATPαS[b,c]	ND[d]	0.58 ± 0.05
	2′-dATP	284 ± 59	0.80 ± 0.06
	2′-dATPαS[c]	ND[d]	0.13 ± 0.01
	2-APTP[e]	85 ± 23	1.95 ± 0.17
	3′-dATP	317 ± 51	1.4 ± 0.1
	GTP	208 ± 66	0.010 ± 0.001
	GTPαS	204 ± 16	(4.1 ± 0.3) × 10^{-3}
sym/sub-UA			
GC**A**UGGGCCCA	UTP	407 ± 43	318 ± 18
ACCCGGGU**A**CG			
sym/sub-A			
GCU**A**GGGCCC	UTP	98 ± 2	266 ± 2
CCCGGG**A**UCG			
sym/sub-C			
GAU**C**GGGCCC	GTP	3.8 ± 0.7	57 ± 3
CCCGGG**C**UAG			
sym/sub-G			
CAU**G**CCCGGG	CTP	19 ± 3	157 ± 8
GGGCCC**G**UAC			

[a] Experiments were performed as described in the legend to Figure 1. [b] Determined at a pH value of 4.5. [c] The observed rate constant for nucleotide incorporation was determined at a concentration of 1 mM nucleotide. [d] Not determined. [e] 2-Aminopurine triphosphate.

Scheme 1: Minimal Kinetic Mechanism for 3D^{pol}-Catalyzed Nucleotide Incorporation[a]

$$ER_n + NTP \underset{}{\overset{K_{d,app}}{\rightleftharpoons}} ER_nNTP \xrightarrow{k_{pol}} ER_{n+1}$$

[a] Abbreviations: ER_n, 3D^{pol} sym/sub complex; NTP, nucleotide; ER_nNTP, ternary complex; $ER_{n+1}PP_i$, product complex.

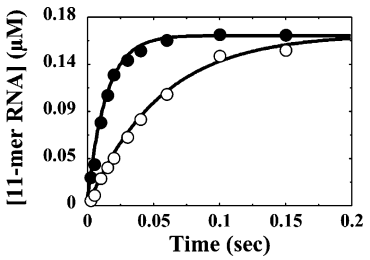

FIGURE 2: Elemental effect on the pre-steady-state rate of AMP incorporation. 2 μM 3D^{pol} was incubated with 2 μM sym/sub (1 μM duplex) and rapidly mixed with either 500 μM ATP (●) or 500 μM ATPαS (○) (final concentration) as described under Experimental Procedures. The solid lines represent the fit of the data to a single exponential with a k_{obs} for ATP of 66.7 ± 1.7 s^{-1} and a k_{obs} for ATPαS of 17.6 ± 0.4 s^{-1}.

obtain a true value for the elemental effect in order to interpret our data. We reasoned that by reducing the pH of the reaction, chemistry should become the rate-limiting step, thereby permitting direct measurement of the elemental effect. We first analyzed the kinetics of nucleotide incorporation at pH values ranging from 4.5 to 8.5. These data gave a pH-independent rate of 108 ± 3 s^{-1} and two pK_a values: 7.0 ± 0.4 and 8.0 ± 0.4. We chose to evaluate the reaction further at pH 4.5. The $K_{d,app}$ and k_{pol} values decreased by 17- and 104-fold, respectively (Table 1). Unexpectedly, the elemental effect observed at this pH was 1.4, a value lower

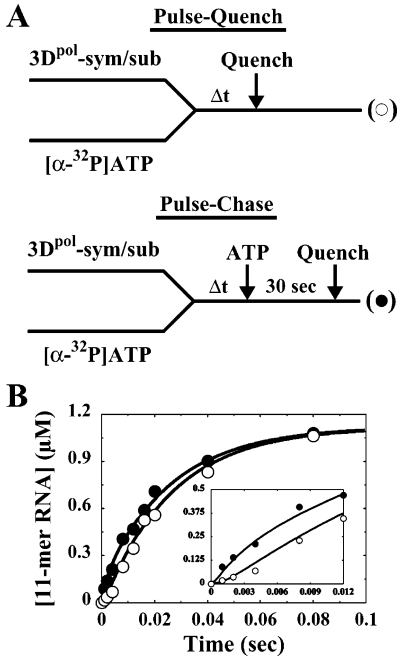

FIGURE 3: Intermediate identification by pulse−chase analysis. (A) Experimental design. 4 μM 3D^{pol} was incubated with 20 μM sym/sub (10 μM duplex) and rapidly mixed with 130 μM [α-^{32}P]ATP (3.8 Ci/mmol) (final concentration) as described under Experimental Procedures. At the indicated times, reactions were either chased by addition of ATP to a final concentration of 20 mM or quenched by addition of HCl to a final concentration of 1 M. After addition of the chase solution, the reaction was allowed to proceed for an additional 30 s, at which time the reaction was quenched by addition of HCl to a final concentration of 1 M. Immediately after addition of HCl, the solution was neutralized by addition of 1 M KOH and 300 mM Tris (final concentration). (B) Kinetics of pulse−chase (●) and pulse−quench (○) from the reactions described in (A). The solid lines represent the kinetic simulation of the data fit to the mechanism shown in Scheme 2 with the kinetic parameters shown in Table 2. The simulated curve of the pulse−quench data predicts the rate of formation of all R_{n+1}-containing species; the simulated curve of the pulse−chase data predicts the rate of formation of *ER_nNTP and all R_{n+1}-containing species.

than that measured at pH 7.6, suggesting that the conformational-change step becomes even more rate limiting at low pH. It is worth noting that reactions performed at the lower values of pH accumulated an intermediate that could not be quenched by using EDTA. Therefore, HCl was employed as a quench for these experiments.

Concurrent with the evaluation of 3D^{pol}-catalyzed nucleotide incorporation in the presence of Mg^{2+}, we were also performing similar studies in the presence of Mn^{2+}. This work is described in detail in the accompanying paper (*33*). Interestingly, in the presence of Mn^{2+}, phosphoryl transfer was shown to be the rate-limiting step for nucleotide incorporation. Under these conditions, an elemental effect of 7.9 was observed. Therefore, we conclude that a conformational change is at least partially rate limiting for nucleotide incorporation in the presence of Mg^{2+}.

To obtain additional evidence for the existence of an isomerized ternary complex, we performed a pulse−quench/pulse−chase experiment (Figure 3A) (*27*, *31*, *34*). This experiment evaluates the kinetics of incorporation of an α-^{32}P-labeled nucleotide into unlabeled primer/template. In the first experiment, the reactants are mixed, and at various times after mixing, the reaction is quenched. In the second

experiment, the reactants are mixed, and at various times after mixing, a chase solution (150-fold molar excess of unlabeled nucleotide) is added; after a time sufficient for incorporation of any trapped, labeled nucleotide (30 s), the reaction is quenched. If an isomerized ternary complex does not exist, then the kinetics of nucleotide incorporation will be the same in both experiments. However, if an isomerized ternary complex does exist, then during the chase, additional product will be produced owing to the inability of the labeled nucleotide associated with this complex to be diluted by the unlabeled nucleotide. The result of this experiment is shown in Figure 3B. The data are consistent with the presence of an isomerized ternary complex.

The pulse−quench experiment showed a lag in product formation, consistent with a rate-limiting conformational change preceding phosphoryl transfer. In addition, the observation of a lag suggests that the rates of the conformational change and phosphoryl transfer are similar. We performed the pulse−quench experiment at three different concentrations of ATP (50, 100, and 130 μM) and obtained the same results (data not shown). By fitting the pulse−quench data to an equation describing a two-step, irreversible process (eq 3), we obtained two apparent rate constants. One apparent rate constant changed as a function of ATP concentration and the other constant did not. We assigned the ATP concentration-independent rate to the chemical step, whose rate constant was 520 ± 200 s^{-1}. Analytical fits of the isotope-trapping experiment then provided estimates for k_{+2} and k_{+3}. Kinetic simulation was then used to identify k_{-2}, leading to a value of 0.6 for K_2.

An alternative approach to determine the value for K_2 was also employed. Given the maximal rate constant for nucleotide incorporation, k_{pol}, the observed elemental effect, E_{obs}, the rate constant for the chemical step, k_{chem}, and the maximal elemental effect, σ, it was possible to use eqs 4−6 to calculate the value for the equilibrium constant across the conformational-change step. This value was also 0.6. Therefore, two approaches, one that was independent of interpretation of the phosphorothioate effect and one that was dependent on the interpretation of the phosphorothioate effect, yield the same value for K_2 and provide compelling evidence that the maximal phosphorothioate effect in the presence of Mg^{2+} is 7.9. This information permitted us to use eq 7 to calculate the true K_d value for ATP dissociating from the $3D^{pol}$−sym/sub−ATP complex; this value was 214 μM. Collectively, these data provide three of the four constraints necessary to describe the results of the pulse−quench/pulse−chase experiment. Kinetic simulation was employed to set a limit on the missing value, the rate constant for the reverse of the chemical step, and values for the rate constants governing the formation and stability of the isomerized ternary complex.

Characterization of the Reverse Reaction. To complete the mechanism, it was necessary to characterize the reverse reaction, pyrophosphorolysis. In the first experiment, we evaluated the dependence of the kinetics of [α-^{32}P]ATP production from sym/sub containing [α-^{32}P]AMP on the concentration of PP_i. The design of this experiment is shown in Figure 4A. The $3D^{pol}$−sym/sub product complex was established by assembling the $3D^{pol}$−sym/sub complex and incorporating [α-^{32}P]AMP into this complex. This mixture was supplemented with Mg^{2+}, which was added first instead

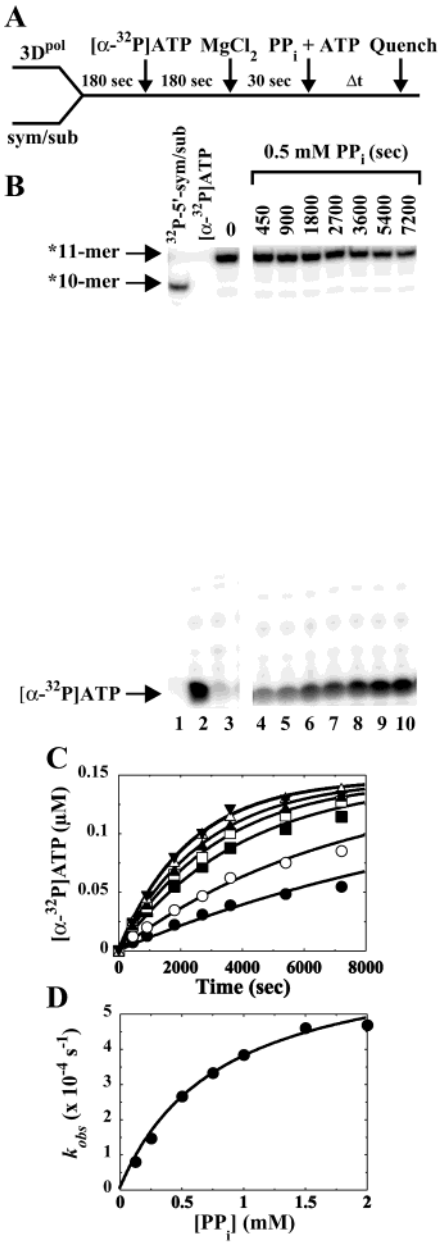

FIGURE 4: Single-turnover pyrophosphorolysis. (A) Experimental design. 2 μM $3D^{pol}$ was incubated with 2 μM sym/sub (1 μM duplex) for 180 s, at which point 0.30 μM [α-^{32}P]ATP (3000 Ci/mmol) was added to the reaction. 180 s after addition of [α-^{32}P]-ATP, supplemental $MgCl_2$ was added to the reaction such that upon addition of PP_i and ATP the final concentration of free $MgCl_2$ was 5 mM. After addition of $MgCl_2$, the reaction was initiated by addition of 100 μM ATP and either 0.125, 0.25, 0.5, 0.75, 1, 1.5, or 2.0 mM PP_i (final concentrations). After mixing, reactant concentrations were reduced by 50%. At fixed times after addition of PP_i and ATP the reaction was quenched by addition of EDTA to a final concentration of 250 mM. (B) Products from a reaction described in (A) at 0.5 mM PP_i (final concentration) resolved by electrophoresis on a denaturing, highly cross-linked 25% polyacrylamide gel. ^{32}P-5′-end-labeled sym/sub and [α-^{32}P]ATP are indicated as a reference (lanes 1 and 2, respectively). (C) Kinetics of pyrophosphorolysis from the reactions described in (A) by monitoring the production of [α-^{32}P]ATP at PP_i concentrations (final) of 0.125 (●), 0.25 (○), 0.5 (■), 0.75 (□), 1.0 (▲), 1.5 (△), and 2.0 mM (▼). The solid lines represent the kinetic simulation of the mechanism shown in Scheme 2 with the kinetic parameters shown in Table 2. (D) k_{obs} as a function of PP_i concentration obtained from the reactions described in (C). The solid line represents the fit of the data to a hyperbola with a $K_{d,app}$ for PP_i of 0.81 ± 0.10 mM and a k_{pryo} of (6.9 ± 0.4) × 10^{-4} s^{-1}.

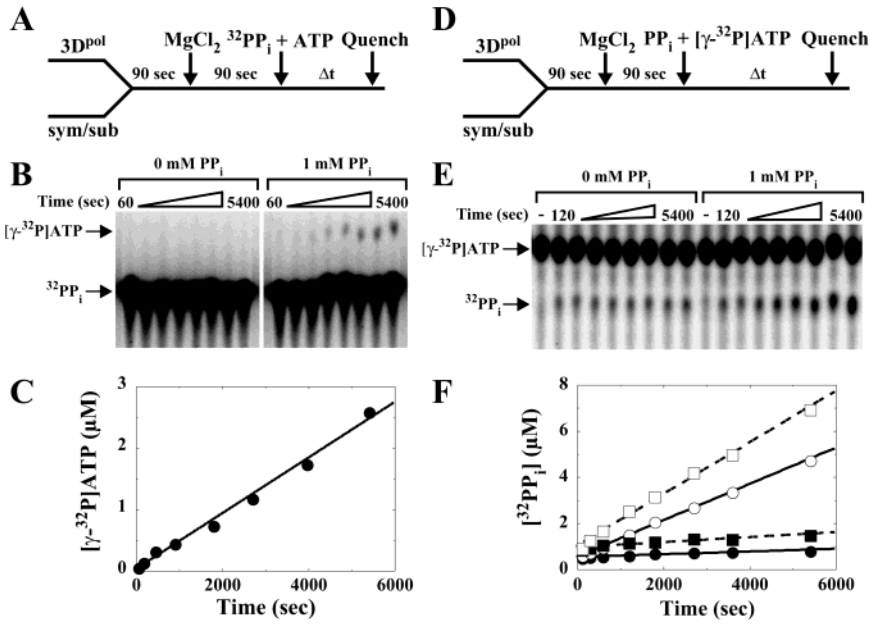

FIGURE 5: Pyrophosphate exchange. (A) Experimental design. 2 μM 3D^{pol} was incubated with 20 μM sym/sub (10 μM duplex) for 90 s to produce 3D^{pol}−sym/sub complexes (0.8 μM), at which point supplemental $MgCl_2$ was added to the reaction such that upon addition of PP_i and ATP the final concentration of free $MgCl_2$ was 5 mM. After addition of $MgCl_2$, the reaction was initiated by addition of 1000 μM ATP and either 0 or 2 mM [^{32}P]PP_i (0.26 Ci/mmol). After mixing, reactant concentrations were reduced by 50%. Reactions were quenched at the indicated times by addition of EDTA to a final concentration of 125 mM. (B) Products from the reactions described in (A) resolved by TLC. (C) Kinetics of pyrophosphate exchange by monitoring the production of [α-^{32}P]ATP at 1 mM PP_i (final concentration). The solid line represents the fit of the data to a line with a *y*-intercept of 0.014 ± 0.005 μM and a slope of (4.52 ± 0.17) × 10^{-4} μM s^{-1}. (D) Experimental design. 2 μM 3D^{pol} was incubated with either 2 or 20 μM sym/sub (1 or 10 μM duplex) for 90 s to produce 3D^{pol}−sym/sub complexes (0.27 or 0.89 μM), at which point supplemental $MgCl_2$ was added to the reaction such that upon addition of PP_i and ATP the final concentration of free $MgCl_2$ was 5 mM. After addition of $MgCl_2$, the reaction was initiated by addition of 200 μM [γ-^{32}P]ATP (10 Ci/mmol) and either 0 or 2 mM PP_i. After mixing, reactant concentrations were reduced by 50%. Reactions were quenched at the indicated times by addition of EDTA to a final concentration of 125 mM. (E) Products from the reactions described in (D) resolved by TLC. (F) Kinetics of pyrophosphate exchange by monitoring the production of [^{32}P]PP_i at 0 (●) and 1 mM (○) PP_i (solid line) for 1 μM sym/sub final and at 0 (■) and 1 mM (□) PP_i (dashed line) for 10 μM sym/sub final. The solid line represents the fit of the data to a line with a *y*-intercept of 0.51 ± 0.02 μM and a slope of (5.9 ± 0.8) × 10^{-5} μM s^{-1} for 0 mM PP_i (1 μM sym/sub final), a *y*-intercept of 0.51 ± 0.03 μM and a slope of (7.8 ± 0.1) × 10^{-4} μM s^{-1} for 1 mM PP_i (1 μM sym/sub final), a *y*-intercept of 0.93 ± 0.04 μM and a slope of (1.1 ± 0.2) × 10^{-4} μM s^{-1} for 0 mM PP_i (10 μM sym/sub final), and a *y*-intercept of 0.98 ± 0.09 μM and a slope of (1.1 ± 0.3) × 10^{-3} μM s^{-1} for 1 mM PP_i (10 μM sym/sub final).

of the PP_i solution in order to prevent precipitation. Next, we added a solution of PP_i and ATP. The presence of ATP prevents the reaction from reaching a premature equilibrium resulting from reincorporation of liberated [α-^{32}P]ATP. The reaction was quenched at various times by addition of EDTA. That the 11-nucleotide product was formed under the conditions employed is readily determined by electrophoresis of the mixture through a highly cross-linked, denaturing polyacrylamide gel followed by phosphorimaging (compare lane 1 to lane 3 in Figure 4B). In addition, we observe stoichiometric utilization of the input [α-^{32}P]ATP (compare lane 2 to lane 3 in Figure 4B); therefore, the error associated with quantifying liberated [α-^{32}P]ATP is very low.

We evaluated the kinetics of pyrophosphorolysis at concentrations of PP_i ranging from 0.125 to 2 mM (the limit of solubility of Mg_2PP_i). The kinetics of pyrophosphorolysis were monophasic, consistent with a conformational change preceding the chemical step limiting the rate of pyrophosphorolysis (*27*, *31*, *34*). Each time course (Figure 4C) was fit to an equation describing a single exponential process (data not shown). The observed rate constant was plotted as function of PP_i concentration and fit to a hyperbola (Figure 4D). The $K_{d,app}$ value for PP_i was 810 μM, and the value for the maximal observed rate constant for pyrophosphorolysis was 6.9 × 10^{-4} s^{-1}.

To determine from which complex PP_i dissociates, we performed a PP_i exchange experiment. This experiment also analyzes the reverse reaction; however, the 3D^{pol}−sym/sub−product complex is formed in the presence of PP_i. Therefore, if PP_i is released prior to the conformational change, then under these experimental conditions, this complex will be accessible to PP_i, giving rise to a difference between the kinetics of PP_i exchange and that of pyrophosphorolysis. For example, the kinetics of PP_i exchange will appear biphasic, and/or the observed rate constant for PP_i exchange may be substantially faster than that of pyrophosphorolysis. The experiment was performed initially by using [^{32}P]PP_i and ATP (Figure 5A) and following production of [γ-^{32}P]ATP by thin-layer chromatography on poly(ethylenimine)−cellulose plates (Figure 5B). A linear accumulation of [γ-^{32}P]-ATP was observed at a rate constant of 4.5 × 10^{-4} μM s^{-1} (Figure 5C). Under the conditions employed, 0.8 μM 3D^{pol}−sym/sub−product complex should have formed; therefore, the rate constant for PP_i exchange was 5.7 × 10^{-4} s^{-1}. A value of 3.1 × 10^{-4} s^{-1} was expected on the basis of the pyrophosphorolysis experiment described above. The observed 2-fold difference could reflect a difference in the actual concentration of 3D^{pol}−sym/sub−product complexes formed in this experiment.

Scheme 2: Complete Kinetic Mechanism for $3D^{pol}$-Catalyzed Nucleotide Incorporation[a]

$$ER_n + NTP \underset{k_{-1}}{\overset{k_{+1}}{\rightleftharpoons}} ER_nNTP \underset{k_{-2}}{\overset{k_{+2}}{\rightleftharpoons}} {}^*ER_nNTP \underset{k_{-3}}{\overset{k_{+3}}{\rightleftharpoons}} {}^*ER_{n+1}PP_i \underset{k_{-4}}{\overset{k_{+4}}{\rightleftharpoons}} ER_{n+1}PP_i \underset{k_{-5}}{\overset{k_{+5}}{\rightleftharpoons}} ER_{n+1} + PP_i$$

[a] Abbreviations: ER_n, $3D^{pol}$ sym/sub complex; NTP, nucleotide; ER_nNTP, ternary complex; $*ER_nNTP$, activated elongation complex; $*ER_{n+1}PP_i$, activated product complex; $ER_{n+1}PP_i$, product complex; ER_{n+1}, $3D^{pol}$ sym/sub product complex; PP_i, pyrophosphate.

To perform the PP_i exchange experiment under conditions in which the concentration of $3D^{pol}$−sym/sub complexes employed could be measured empirically, we performed the experiment by using PP_i and [γ-^{32}P]ATP (Figure 5D), following production of [^{32}P]PP_i by TLC (Figure 5E). This approach gives a burst of [^{32}P]PP_i production equivalent to the concentration of active $3D^{pol}$−sym/sub complexes formed. A burst of [^{32}P]PP_i formation was observed in the absence (0.51 μM) and presence (0.51 μM) of added PP_i for 1 μM sym/sub-U, and a burst of [^{32}P]PP_i formation was observed in the absence (0.93 μM) and presence (0.89 μM) of added PP_i for 10 μM sym/sub-U (Figure 5F). The expected burst amplitude was 0.27 μM for 1 μM sym/sub-U and 0.89 μM for 10 μM sym/sub-U. In the presence of PP_i, [^{32}P]PP_i accumulated at a rate constant of 7.8×10^{-4} μM s^{-1} and 1.1×10^{-3} μM s^{-1} for 1 and 10 μM sym/sub-U, respectively. The corresponding rate constant for PP_i exchange was 2.9×10^{-3} s^{-1} and 1.2×10^{-3} s^{-1}; these values are 7- and 3-fold greater than expected. This experiment was repeated several times under a variety of conditions, and in all cases there was a 3−7-fold increase in the rate constant for PP_i exchange relative to the value calculated from the parameters obtained by evaluating the kinetics of pyrophosphorolysis. However, in no case was there a significant difference in the burst amplitude measured in the absence and presence of PP_i.

These data can be explained in three different ways. First, it is possible that PP_i can dissociate from ~1% of the $3D^{pol}$−sym/sub−product complexes prior to undergoing a second conformational change. The value of 1% was calculated by assuming that the fraction of enzyme accessible to PP_i before the second conformational-change step should undergo PP_i exchange at a rate dictated by the rate constant for the reverse of the chemical step (375 s^{-1}). Second, there may be two steps after chemistry: a conformational-change step, which permits PP_i release, and a conformational-change step that translocates the enzyme into position for the next cycle of nucleotide incorporation. The latter step would be measured in the pyrophosphorolysis experiment; both steps would be accessible during the PP_i exchange experiment. Third, it is possible that a 3−7-fold difference between the rate constants for PP_i exchange and pyrophosphorolysis is not a significant difference and reflects error associated with comparing rate constants obtained by using the two different experimental protocols despite the observed reproducibility of each experimental approach. Regardless of the precise explanation for the increase in the rate of PP_i exchange relative to pyrophosphorolysis, all of the possibilities described above are consistent with PP_i dissociating from a complex that has undergone a conformational change after chemistry. If PP_i were released from the internal complex prior to the conformational change, then one would expect PP_i exchange to occur at a rate on the order of 375 s^{-1} that is dictated by phosphoryl transfer. This value is >500000-fold faster than pyrophosphorolysis. So, the observed 3−7-fold difference can in no way be misconstrued as a substantial fraction of PP_i dissociating from an internal complex.

Table 2: Kinetic Parameters for the Kinetic Mechanism of $3D^{pol}$-Catalyzed Nucleotide Incorporation (Scheme 2)

parameter	value[a]	K_{eq}
k_{+1}	10 μM^{-1} s^{-1}	
k_{-1}	2140 s^{-1}	4.7×10^{-3} μM^{-1}
k_{+2}	300 s^{-1}	
k_{-2}	500 s^{-1}	0.6
k_{+3}	520 s^{-1}	
k_{-3}	375 s^{-1}	1.4
k_{+4}	500 s^{-1}	
k_{-4}	0.0025 s^{-1}	2.0×10^5
k_{+5}	8100 s^{-1}	
k_{-5}	10 μM^{-1} s^{-1}	810 μM

[a] Values for all parameters, with the exception of k_{-3}, were determined experimentally.

Additional Evidence for a Conformational Change after Nucleotide Incorporation. The monophasic nature of the kinetics of pyrophosphorolysis suggests that a conformational-change step exists after the phosphoryl-transfer step (*27*, *31*, *34*). The existence of this conformational-change step is also supported by the PP_i exchange experiments. To obtain additional evidence for the existence of this step and to determine whether this step modulates the efficiency of subsequent cycles of nucleotide incorporation, we performed an experiment evaluating two consecutive cycles of nucleotide incorporation. In this experiment, $3D^{pol}$−sym/sub complexes were assembled and mixed with ATP (500 μM) in the absence or presence of varying concentrations of UTP (100, 300, and 1000 μM). The data were simulated with a two-step, irreversible process, yielding in each case a rate constant for AMP incorporation of 70 s^{-1} and rates of UMP incorporation of 25, 50, and 60 s^{-1} at 100, 300, and 1000 μM UTP, respectively. By plotting the observed rates of UMP incorporation as a function of UTP concentration and fitting these data to a hyperbola, we obtained a $K_{d,app}$ value for UTP of 159 ± 55 μM and a k_{pol} value of 71 ± 7 s^{-1}. This k_{pol} value was significantly different than the value of 317 s^{-1} measured by evaluation of UMP incorporation into a $3D^{pol}$−sym/sub product complex (see sym/sub-UA in Table 1), suggesting that a step after incorporation of the first nucleotide likely attenuates the rate of incorporation of the second nucleotide. If we fit these data to the mechanism for AMP incorporation shown in Scheme 2 using the parameters shown in Table 2 and link this to the mechanism shown in Scheme 1 to describe UMP incorporation by using the parameters for UMP incorporation into sym/sub-UA shown in Table 1, then we get a good fit of the data for the two-nucleotide incorporation experiment by using a rate constant of 500 s^{-1} for the conformational change after incorporation of AMP (Figure 6A). The data for 1000 μM ATP are omitted for clarity. That the rate constant for this conformational change modulates the observed rate constant for incorporation of the next nucleotide is also supported by the experiment shown in Figure 6B. In the simulations for this experiment, we show that a 4−5-fold change in the rate constant for the conformational-change step after nucleotide

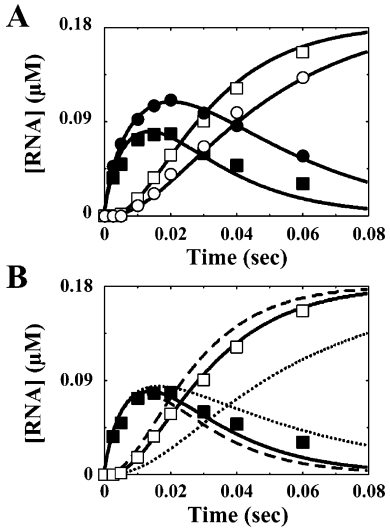

FIGURE 6: Evidence for a conformational change after chemistry. (A) 2 μM 3D^{pol} was incubated with 2 μM sym/sub (1 μM duplex) and rapidly mixed with 500 μM ATP and either 100 or 300 μM UTP (final concentrations). After mixing, reactant concentrations were reduced by 50%. Key: Kinetics of formation and disappearance of the 11-mer (●) and 12-mer (○) for 500 μM ATP and 100 μM UTP (final) and kinetics of formation and disappearance of the 11-mer (■) and 12-mer (□) for 500 μM ATP and 300 μM UTP (final). The solid lines represent the kinetic simulation of the data fit to a mechanism for two successive nucleotide incorporations with the first nucleotide incorporation described by the kinetic mechanism shown in Scheme 2 using the kinetic parameters in Table 2 and the second nucleotide incorporation described by the mechanism shown in Scheme 1 using the $K_{d,app}$ and k_{pol} values for UTP using sym/sub-UA shown in Table 1. (B) Kinetics of formation and disappearance of the 11-mer (■) and 12-mer (□) for the reaction described in (A) for 500 μM ATP and 300 μM UTP (final). The lines represent the kinetic simulation of the data fit to a mechanism for two successive nucleotide incorporations with the first nucleotide incorporation described by the kinetic mechanism shown in Scheme 2 using the kinetic parameters in Table 2 and the second nucleotide incorporation described by the mechanism shown in Scheme 1 using the $K_{d,app}$ and k_{pol} values for UTP using sym/sub-UA shown in Table 1, however with different values for k_{+4}. The solid line is the fit of the data with a k_{+4} of 500 s^{-1}, the longer dashed line is the fit of the data with a k_{+4} of 2000 s^{-1}, and the smaller dashed line is the fit of the data with a k_{+4} of 100 s^{-1}.

incorporation significantly alters the fit of the simulation to the data (Figure 6B). This experiment also provides good constraints on the rate constant for this step.

Processive Synthesis. To determine whether all cycles of nucleotide incorporation are equivalent, we performed an experiment evaluating incorporation of all four nucleotides. The results are shown in Figure 7. As expected, all cycles are equivalent and additional barriers to nucleotide incorporation do not exist. Each cycle could be described by the same rate constant of 50 s^{-1}. This value is predicted for incorporation of the first nucleotide, ATP (Table 1), and predicted values for the subsequent incorporation steps are 121 s^{-1} (UTP), 56 s^{-1} (GTP), and 146 s^{-1} (CTP), based upon the kinetics of incorporation of each individual nucleotide presented in Table 1. These data are consistent with the conformational-change step after chemistry limiting the rate of incorporation of each nucleotide as discussed above.

Nucleotide Specificity of 3D^{pol}. The final set of experiments was designed to obtain some information on the mechanism employed by 3D^{pol} to select for nucleotides with the correct sugar configuration and the correct base. For DNA polymerases and reverse transcriptases, selection against incorporation of ribonucleotides is facilitated by the existence of residues in the nucleotide-binding pocket that create a steric block for the 2′-OH of the rNTP, manifesting in a large increase in the K_d value for an rNTP with a correct base relative to the correct 2′-dNTP (*30*). Significant increases in K_d values are also observed for nucleotides with the incorrect base (*5*, *30*). In contrast, loss of the 3′-OH in these systems is manifested as a reduction in the k_{pol} value for incorporation without significant differences in the K_d value (*5*, *29*, *35*). As shown in Table 1 for the sym/sub-U substrate, the apparent dissociation constant of nucleotides with an incorrect sugar configuration (2′-dATP and 3′-dATP), an incorrect base (GTP), or a change in the location of the base-template hydrogen bonds (2-APTP) were all very similar to each other and 2−3-fold weaker than ATP. However, substantial decreases (40−100-fold) in the observed rate constant for incorporation existed (Table 1). Particularly intriguing was the observation that 2-aminopurine also showed a reduction in the observed rate constant for incorporation relative to ATP. The only difference between these two nucleotides is the position of the amino group. This difference changes the location of one hydrogen bond from the major groove (ATP) to the minor groove (2-APTP), suggesting that 3D^{pol} may have specific side chains interacting with the nascent base pair in the major groove that facilitate formation of a catalytically competent ternary complex.

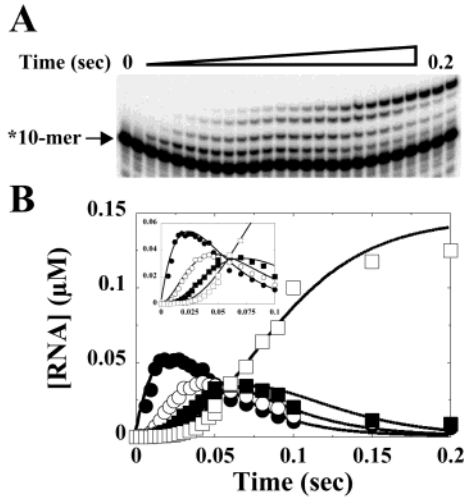

FIGURE 7: Processive synthesis of ribonucleotide incorporation into sym/sub. (A) 2 μM 3D^{pol} was incubated with 2 μM sym/sub (1 μM duplex) and rapidly mixed with 250 μM each NTP. (B) Kinetics of formation and disappearance of 11-mer (●), 12-mer (○), 13-mer (■), and 14-mer (□). The solid lines represent the kinetic simulation of the data fit to four sequential nucleotide incorporations with net rate constants for formation of 11-mer at 50 s^{-1}, 12-mer at 50 s^{-1}, 13-mer at 50 s^{-1}, and 14-mer at 50 s^{-1}.

DISCUSSION

Complete Kinetic Mechanism for 3D^{pol}-Catalyzed Single Nucleotide Incorporation. The experimental data are consistent with the mechanism shown in Scheme 2 governed by the rate constants shown in Table 2. The 3D^{pol}−sym/sub complex (ER_n) binds nucleotide (NTP) to form a ternary complex (ER_nNTP) that isomerizes to form a complex that is competent for phosphoryl transfer ($*ER_nNTP$). Chemistry occurs, forming a ternary product complex ($*ER_{n+1}PP_i$); this

Table 3: Values for the Rate Constants Employed in Kinetic Simulations Are Constrained by Experimental Data[a]

experiment	2-fold change	10-fold change	insensitive
kinetics of AMP incorporation	k_{+1}, k_{-1}, k_{+2}, k_{-2},[b] k_{+3},[c] k_{-3}[a]	k_{-2}, k_{+3}, k_{-3}, k_{+4}	k_{-4}, k_{+5}, k_{-5}
pulse−chase analysis	k_{+1}, k_{-1}, k_{+2}, k_{-2}, k_{+3}, k_{-3}[b]	k_{-3}, k_{+4}	k_{-4}, k_{+5}, k_{-5}
pyrophosphorolysis	k_{-2}, k_{+3}, k_{-3}, k_{+4}, k_{-4}, k_{+5}, k_{-5}	k_{+1},[d] k_{-1},[e] k_{+2}[d]	
two-nucleotide incorporation	k_{+1}, k_{-1}, k_{+2}, k_{-2}, k_{+3}, k_{+4}[b]	k_{-3}, k_{+4}, $K_{d,app,UTP}$, $k_{pol,UTP}$	k_{-4}, k_{+5}, k_{-5}

[a] The rate constants shown in Table 2 were increased or decreased by 2- or 10-fold, and the fit of the simulation to the indicated experimental data was evaluated. In most instances, either an increase or decrease in the indicated rate constants altered the goodness of fit. However, exceptions were noted, and these are annotated to indicate this fact. Finally, rate constants that can be varied by greater than 10-fold without any apparent change in the fit of the simulation to the data are indicated in the column labeled insensitive. [b] Only a 2-fold increase gives a significant change in the fit of the simulation to the data. [c] Only a 2-fold decrease gives a significant change in the fit of the simulation to the data. [d] Only a 10-fold increase gives a significant change in the fit of the simulation to the data. [e] Only a 10-fold decrease gives a significant change in the fit of the simulation to the data.

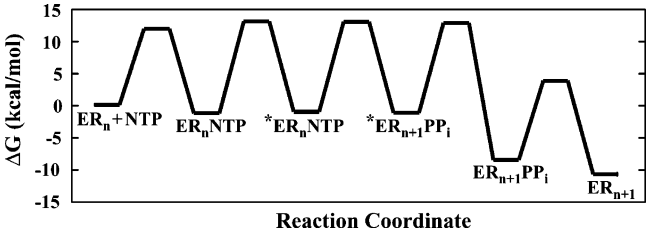

FIGURE 8: Free energy profile for 3D^{pol}-catalyzed nucleotide incorporation. The free energy changes for nucleotide incorporation were calculated from the kinetic parameters shown in Table 2. The concentrations of the substrates and products used were 2000 μM ATP and 20 μM PP_i. The free energy for each reaction step was calculated from $\Delta G = RT[\ln(kT/h) - \ln(k_{obs})]$, where R is 1.99 cal K^{-1} mol^{-1}, T is 303 K, k is 3.30×10^{-24} cal K^{-1}, h is 1.58×10^{-34} cal s, and k_{obs} is the first-order rate constant. The free energy for each species was calculated from $\Delta G = RT[\ln(kT/h) - \ln(k_{obs,for})] - RT[\ln(kT/h) - \ln(k_{obs,rev})]$.

complex undergoes a second conformational change to form a ternary product complex ($ER_{n+1}PP_i$) from which PP_i can dissociate. After dissociation of PP_i, a 3D^{pol}−sym/sub product complex (ER_{n+1}) remains that is competent for the next cycle of nucleotide incorporation. Experimental evidence has been obtained for each step in this mechanism, including each conformational-change step (Figures 1−7). The kinetic parameters shown in Table 2 were either determined empirically or calculated. That this single set of rate constants accurately describes 3D^{pol}-catalyzed incorporation of AMP into sym/sub-U is supported by kinetic simulation. The ATP concentration dependence of the kinetics of AMP incorporation (Figure 1), the pulse−chase analysis (Figure 3), the PP_i concentration dependence of the kinetics of pyrophosphorolysis (Figure 4), and the kinetics of two consecutive cycles of nucleotide incorporation (Figure 6) are all simulated by the mechanism shown in Scheme 2 and the single set of rate constants presented in Table 2. Moreover, none of the forward or reverse rate constants could be changed by more than 2-fold without causing a visually observable deviation in the goodness of fit of the simulation to at least one set of experimental data (Table 3). A 10-fold change in any kinetic parameter affected the goodness of fit of the simulation to most sets of experimental data (Table 3); a few exceptions were noted (Table 3).

The free energy profile for the reaction is shown in Figure 8. Physiological concentrations of ATP (2 mM) and PP_i (20 μM) were employed in the calculations (*36*, *37*). The overall free energy change for single nucleotide incorporation is −10.8 kcal/mol. All steps from formation of the first ternary complex to formation of the first product complex are isoenergetic. The stability of each intermediate of the pathway is ∼−1.0 kcal/mol, and each activation barrier is approximately 14.0 kcal/mol. The largest free energy change results from the conformational change after phosphoryl transfer (−7.3 kcal/mol). This step renders correct nucleotide incorporation essentially irreversible. An additional free energy change of −2.2 kcal/mol occurs after PP_i release.

Comparison of the Mechanism for 3D^{pol}-Catalyzed Nucleotide Incorporation to Mechanisms for Other Nucleic Acid Polymerases. The sequence of steps employed by 3D^{pol} is identical to that employed by the reverse transcriptase from human immunodeficiency virus (*5*, *31*) and DNA polymerases from *Escherichia coli* [Klenow fragment (KF) of DNA polymerase I] (*28*, *34*) and bacteriophage T7 (*27*). Two primary differences exist between 3D^{pol} and the other polymerases. First, the rate of phosphoryl transfer is partially limiting for 3D^{pol}-catalyzed nucleotide incorporation. For the DNA polymerases, it has been suggested that phosphoryl transfer is very fast relative to the first conformational-change step and does not present an impediment to reaction progress. Second, the magnitude of the free energy change associated with the second conformational-change step is greater for 3D^{pol} (−7.3 kcal/mol) than for T7 DNA polymerase (−2.4 kcal/mol) (*27*) and KF (0 kcal/mol) (*34*). In the case of KF, the largest free energy change occurs across the first conformational-change step (∼−2.0 kcal/mol) (*34*). It should be noted that estimation of the value of the rate constant for phosphoryl transfer is dependent upon the ability to interpret the observed phosphorothioate elemental effect (see eq 4). If one assumes that the maximal elemental effect for all polymerases is in the range of 7.9, then phosphoryl transfer may be partially rate limiting for all polymerases studied to date.

Conformational Changes during 3D^{pol}-Catalyzed Nucleotide Incorporation. A distinct feature of all nucleic acid polymerases studied to date is the existence of conformational changes before and after phosphoryl transfer (*27*, *34*). These steps are also present in the kinetic mechanism for 3D^{pol}. In the first reports on KF, it was suggested that the first conformational change may reflect reorientation of the triphosphate moiety of the incoming nucleotide to interact with side chains of the enzyme (*28*). This hypothesis was put forward to explain the observation made by Mildvan and colleagues that the orientation of the triphosphate and its interaction with divalent cation change in a KF ternary complex (*38*, *39*). Recently, it has been suggested that the conformational change defined kinetically may be related to changes in the orientation of the fingers subdomain

observed crystallographically (*12*, *40*, *41*). We favor the hypothesis that the first conformational change observed kinetically for 3D^{pol} is related to (re)positioning of the triphosphate moiety of the incoming nucleotide in the catalytic and/or nucleotide-binding sites because the first conformational-change step is sensitive to the nature of the divalent cation employed in the reaction (*33*). The triphosphate moiety of the nucleotide is the most likely mediator of this effect.

The second conformational change is likely translocation of the enzyme along template to move into position for the next cycle of nucleotide incorporation. This hypothesis has been put forward for the DNA polymerases (*27*, *34*). Clearly, in the case of 3D^{pol}, this step attenuates both the apparent dissociation constant and the incorporation rate for the second nucleotide (Figure 6). This conformational-change step likely attenuates the rate of all cycles of nucleotide incorporation after the first incorporation (Figure 7). Similar observations have been made with KF (*34*).

Fidelity of 3D^{pol}-Catalyzed Nucleotide Incorporation. One of the primary incentives for performing this study was to provide a kinetic and thermodynamic explanation for the statement made in most of the literature discussing RdRPs that these enzymes have an "extraordinarily high mutation rate" (*42*). Surprisingly, the intrinsic fidelity of 3D^{pol} is similar to that of T7 DNA polymerase (*43*), ranging from 1/15000 for a G·U mispair (Table 1) to <1/150000 for C·U and U·U mispairs (data not shown). These values are at least 10-fold higher than observed for both KF (*44*) and HIV RT (*5*). In contrast to observations made for T7 DNA polymerase (*43*) but similar to observations made for KF (*44*), selection for a nucleotide with an incorrect base does not occur to the greatest extent in the ground state for nucleotide binding. Rather, this selection process occurs both in the ground state for the first conformational-change step and in the transition state for phosphoryl transfer (*44*). This conclusion is based upon the finding that there is only a 2.3-fold increase in the apparent dissociation constant for GTP relative to ATP when sym/sub-U is employed (Table 1), but GTP is incorporated 6700-fold less efficiently than ATP. The same argument can be presented to support the hypothesis that selection against incorporation of nucleotides with an incorrect sugar configuration (2′-dATP and 3′-dATP in Table 1) only involves the first conformational-change step and/or phosphoryl transfer rather than binding.

Because the equilibrium constant across the first conformational-change step is 0.6 (Table 2), a decrease in the stability of this complex will appear as a reduction in the observed rate constant for nucleotide incorporation. For example, it is possible to simulate the kinetics of 2′-dAMP incorporation into sym/sub-U by changing the equilibrium constant across the conformational-change step from 0.6 to 0.006 without any other changes (data not shown). The 100-fold reduction in complex stability is consistent with the loss of a single hydrogen bond. The mechanism for selection of nucleotides with a correct sugar configuration does not require an induced-fit mechanism (*45*) as the rate constant for isomerization of the ternary complex is probably unaffected. The induced-fit mechanism may be reserved for selection against nucleotides with an incorrect base and may be employed by 3D^{pol}. Rigorous evaluation of the kinetic mechanism for incorrect nucleotide incorporation will be required to address this issue. In addition, a precise description of the mechanism employed by 3D^{pol} to couple the nature of the bound nucleotide to the efficiency of catalysis also requires additional studies. It is possible that the initial binding of nucleotide is driven by the triphosphate moiety. If the correct base is present, then the rate of triphosphate repositioning for catalysis may be facilitated by base pairing between the nucleotide and the template. The stability of this "active" conformation could be enhanced by the presence of the correct base pair and a correct sugar configuration.

After nucleotide incorporation, the second conformational-change step could be used as a mechanism for proofreading. For example, the efficiency of translocation into position for the next cycle of nucleotide incorporation may be linked to the nature of the base pairing at the 3′-end of the primer. The enzyme may not be able to bypass a frayed (mispaired) end very efficiently. Increasing the activation barrier for translocation would permit removal of the nucleotide and a second opportunity for nucleotide selection. Indeed, studies with KF have demonstrated that such a mechanism is feasible (*34*).

The ability to evaluate whether the bound nucleotide is correct prior to incorporation should contribute significantly to the fidelity of incorporation. 3D^{pol} may have the capacity to perform this task by interacting with the nascent base pair in the major groove. The incorporation efficiency of 2-aminopurine triphosphate is reduced by 40-fold relative to ATP (Table 1). In both cases, base pairing with uracil should form an interaction that is coplanar with the existing base pairs and stabilized by two hydrogen bonds (*46*). The one difference is that only one hydrogen-bonding interaction of the base pair will be accessible from the major groove when 2-aminopurine is present whereas two hydrogen-bonding interactions will be accessible from the major groove when adenine is present. Additional studies will be required to determine whether this observation reflects an exception or a general rule for 3D^{pol}-catalyzed nucleotide incorporation.

Implications for Development of Antivirals. It is clear from our published work that once 3D^{pol} has initiated RNA synthesis, it is likely that this enzyme will not dissociate from nascent RNA until it reaches the end of the genome (*23*). It is probable that this situation will extend to other RdRPs, especially the enzyme from hepatitis C virus (*47*). Therefore, it is reasonable to target the elongation complex for antiviral drug development. The data reported herein are consistent with a model in which the conformation of the triphosphate moiety mediates information from the base- and sugar-binding pockets to the catalytic center of the enzyme. Domain movements observed crystallographically are likely required for efficient catalysis but may be a consequence of correct positioning of nucleotide in the catalytic site of the enzyme. Hydrogen bonding to the 2′- and 3′-hydroxyl moieties of the ribonucleotide and possibly hydrogen bonding in the major groove of the nascent base pair are important determinants of the conformation and stability of the isomerized ternary complex and key regulators of the efficiency of nucleotide incorporation. Together, these observations suggest that design of antiviral nucleosides may be challenging if multiple incorporation events are required for a biological effect. One possible way to circumvent this problem is the use of analogues containing a pseudobase that permits an active conformation to be achieved with as many of the

nucleobases as possible. Given that RNA viruses exist on the threshold of error catastrophe, the number of incorporation events required to achieve a significant biological effect will be minimal (*48*).

Another important point to consider in the design of antiviral nucleotides is the cellular nucleotide pool with which the antiviral nucleotide competes. The physiological concentrations of nucleotides are 2102 μM ATP, 253 μM UTP, 468 μM GTP, and 91 μM CTP (*37*). Not surprisingly, these values are well above the $K_{d,app}$ values measured for nucleotide incorporation (Table 1). The one nucleotide pool that exists very near, and in some instances below, the $K_{d,app}$ value is UTP (Table 1). Therefore, it is reasonable to conclude that uridine analogues may compete better with normal pools for utilization by the polymerase. In addition, the efficiency of viral RNA synthesis and consequently virus production may be affected quite dramatically by decreasing the intracellular UTP concentration. We have noted that a 2.5−5-fold reduction in the polymerase elongation rate can cause a temperature-sensitive growth phenotype or completely inhibit virus production (*26*). One known antiviral nucleotide, ribavirin monophosphate, decreases GTP pools in cells (*49*), thereby potentiating the mutagenic effect of ribavirin triphosphate on the viral genome (*48*). Inhibitors of enzymes that target de novo uridine biosynthesis may have antiviral activity. Because CTP is produced by transfer of an amino group to the pyrimidine ring of UTP, inhibitors of UTP biosynthesis will also decrease cellular CTP pools. Pyrazofurin, a pyrimidine biosynthesis inhibitor, is more effective against RNA viruses than purine biosynthesis inhibitors (*50*). Given the capacity of pyrazofurin to decrease cellular pyrimidine nucleotide pools, it is possible that a factor contributing to the potent activity of this agent is the sensitivity of the rate of UMP incorporation to subtle changes in UTP concentration caused by the K_d value of UTP being so close to that of the normal cellular concentration. It is worth noting that inhibitors of pyrimidine biosynthesis have been shown to exhibit antiviral activity against Sindbis virus; however, drug-resistant virus with mutations in the polymerase gene rapidly emerged (*50*).

Our kinetic data suggest that the $K_{d,app}$ value for 2′-dATP is 100-fold higher than the physiological concentration of this nucleotide (2.4 μM) (*37*) (Table 1). The cytosolic concentration of 2′-dATP and other 2′-dNTPs may actually be even lower than measured for the total cell as production of this biomolecule occurs predominantly in the nucleus (*37*). Coupled with the 100-fold reduction in the rate of 2′-dAMP incorporation relative to AMP incorporation (Table 1), the frequency of 2′-dAMP incorporation into viral RNA should be <1 per 10000 nucleotides incorporated. Given that the poliovirus genome is only 7500 nucleotides in length, very few genomes, if any, will contain a deoxyribonucleotide. We have noted that incorporation of 2′-dAMP into nascent RNA impedes efficient elongation of RNA; the observed rate constant for incorporation of a ribonucleotide after incorporation of the correct deoxyribonucleotide is reduced by a factor of 10 relative to the normal scenario. Perhaps increasing the cytosolic concentration of dTTP or dCTP will produce an antiviral effect.

Whether any of the ideas discussed above will have clinical applicability remains to be seen. However, some of these ideas should have an immediate, practical utility on our understanding of the structure−function relationships of this class of nucleic acid polymerases. For example, selection for virus that can grow in the presence of inhibitors of pyrimidine biosynthesis should provide insight into the molecular basis for recognition of the nascent base pair by $3D^{pol}$. Selection of virus that can grow in the presence of high concentrations of deoxyribonucleotides will provide additional information on the molecular determinants of ribose selection. In general, this information will provide a more accurate molecular description of the mechanisms contributing to RdRP fidelity.

ACKNOWLEDGMENT

We thank Professor J. Martin Bollinger for very insightful, enthusiastic discussions. We also thank Professor Kevin D. Raney for critical review of the manuscript. Finally, we thank Larry C. Sowers for generously providing 2-aminopurine 5′-triphosphate.

REFERENCES

1. Jonckheere, H., Anne, J., and De Clercq, E. (2000) The HIV-1 reverse transcription (RT) process as target for RT inhibitors, *Med. Res. Rev. 20*, 129−154.
2. Tarrago-Litvak, L., Andreola, M. L., Nevinsky, G. A., Sarih-Cottin, L., and Litvak, S. (1994) The reverse transcriptase of HIV-1: From enzymology to therapeutic intervention, *FASEB J. 8*, 497−503.
3. De Clercq, E. (1992) HIV inhibitors targeted at the reverse transcriptase, *AIDS Res. Hum. Retroviruses 8*, 119−134.
4. Furman, P. A., Painter, G. R., and Anderson, K. S. (2000) An analysis of the catalytic cycle of HIV-1 reverse transcriptase: Opportunities for chemotherapeutic intervention based on enzyme inhibition, *Curr. Pharm. Des. 6*, 547−567.
5. Kati, W. M., Johnson, K. A., Jerva, L. F., and Anderson, K. S. (1992) Mechanism and fidelity of HIV reverse transcriptase, *J. Biol. Chem. 267*, 25988−25997.
6. Spence, R. A., Anderson, K. S., and Johnson, K. A. (1996) HIV-1 reverse transcriptase resistance to nonnucleoside inhibitors, *Biochemistry 35*, 1054−1063.
7. Spence, R. A., Kati, W. M., Anderson, K. S., and Johnson, K. A. (1995) Mechanism of inhibition of HIV-1 reverse transcriptase by nonnucleoside inhibitors, *Science 267*, 988−993.
8. Kohlstaedt, L. A., Wang, J., Friedman, J. M., Rice, P. A., and Steitz, T. A. (1992) Crystal structure at 3.5 A resolution of HIV-1 reverse transcriptase complexed with an inhibitor, *Science 256*, 1783−1790.
9. Jacobo-Molina, A., Ding, J., Nanni, R. G., Clark, A. D., Jr., Lu, X., Tantillo, C., Williams, R. L., Kamer, G., Ferris, A. L., Clark, P., Hizi, A., Hughes, S. H., and Arnold, E. (1993) Crystal structure of human immunodeficiency virus type 1 reverse transcriptase complexed with double-stranded DNA at 3.0 Å resolution shows bent DNA, *Proc. Natl. Acad. Sci. U.S.A. 90*, 6320−6324.
10. Jager, J., Smerdon, S. J., Wang, J., Boisvert, D. C., and Steitz, T. A. (1994) Comparison of three different crystal forms shows HIV-1 reverse transcriptase displays an internal swivel motion, *Structure 2*, 869−876.
11. Rodgers, D. W., Gamblin, S. J., Harris, B. A., Ray, S., Culp, J. S., Hellmig, B., Woolf, D. J., Debouck, C., and Harrison, S. C. (1995) The structure of unliganded reverse transcriptase from the human immunodeficiency virus type 1, *Proc. Natl. Acad. Sci. U.S.A. 92*, 1222−1226.
12. Huang, H., Chopra, R., Verdine, G. L., and Harrison, S. C. (1998) Structure of a covalently trapped catalytic complex of HIV-1 reverse transcriptase: implications for drug resistance, *Science 282*, 1669−1675.
13. Ren, J., Esnouf, R., Garman, E., Somers, D., Ross, C., Kirby, I., Keeling, J., Darby, G., Jones, Y., Stuart, D. I., and Stammers, D. (1995) High-resolution structures of HIV-1 RT from four RT-inhibitor complexes, *Nat. Struct. Biol. 2*, 293−302.
14. Ding, J., Das, K., Tantillo, C., Zhang, W., Clark, A. D., Jr., Jessen, S., Lu, X., Hsiou, Y., Jacobo-Molina, A., Andries, K., Pauwels, R., Moereels, H., Koymans, L., Janssen, P. A. J., Smith, R. H. J., Kroeger Koepke, R., Michejda, C. J., Hughes, S. H., and Arnold,

E. (1995) Structure of HIV-1 reverse transcriptase in a complex with the nonnucleoside inhibitor alpha-APA R 95845 at 2.8 A resolution, *Structure 3*, 365−379.
15. Arts, E. J., and Le Grice, S. F. (1998) Interaction of retroviral reverse transcriptase with template-primer duplexes during replication, *Prog. Nucleic Acid Res. 58*, 339−393.
16. Frankel, A. D., and Young, J. A. (1998) HIV-1: Fifteen proteins and an RNA, *Annu. Rev. Biochem. 67*, 1−25.
17. Davis, W. R., Tomsho, J., Nikam, S., Cook, E. M., Somand, D., and Peliska, J. A. (2000) Inhibition of HIV-1 reverse transcriptase-catalyzed DNA strand transfer reactions by 4-chlorophenylhydrazone of mesoxalic acid, *Biochemistry 39*, 14279−14291.
18. Peliska, J. A., and Benkovic, S. J. (1992) Mechanism of DNA strand transfer reactions catalyzed by HIV-1 reverse transcriptase, *Science 258*, 1112−1118.
19. Peliska, J. A., Balasubramanian, S., Giedroc, D. P., and Benkovic S. J. (1994) Recombinant HIV-1 nucleocapsid protein accelerates HIV-1 reverse transcriptase catalyzed DNA strand transfer reactions and modulates RNase H activity, *Biochemistry 33*, 13817−13823.
20. Cameron, C. E., Ghosh, M., Le Grice, S. F., and Benkovic, S. J. (1997) Mutations in HIV reverse transcriptase which alter RNase H activity and decrease strand transfer efficiency are suppressed by HIV nucleocapsid protein, *Proc. Natl. Acad. Sci. U.S.A. 94*, 6700−6705.
21. Wei, X., Gotte, M., and Wainberg, M. A. (2000) Human immunodeficiency virus type-1 reverse transcription can be inhibited in vitro by oligonucleotides that target both natural and synthetic tRNA primers, *Nucleic Acids Res. 28*, 3065−3074.
22. Thrall, S. H., Reinstein, J., Wöhrl, B. M., and Goody, R. S. (1996) Evaluation of human immunodeficiency virus type 1 reverse transcriptase primer tRNA binding by fluorescence spectroscopy: Specificity and comparison to primer/template binding, *Biochemistry 35*, 4609−4618.
23. Arnold, J. J., and Cameron, C. E. (2000) Poliovirus RNA-dependent RNA polymerase (3D^{pol}): Assembly of stable, elongation-competent complexes by using a symmetrical primer-template substrate (sym/sub), *J. Biol. Chem. 275*, 5329−5336.
24. Gohara, D. W., Ha, C. S., Kumar, S., Ghosh, B., Arnold, J. J., Wisniewski, T. J., and Cameron C. E. (1999) Production of "authentic" poliovirus RNA-dependent RNA polymerase (3D^{pol}) by ubiquitin-protease-mediated cleavage in *Escherichia coli*, *Protein Expression Purif. 17*, 128−138.
25. Hansen, J. L., Long, A. M., and Schultz, S. C. (1997) Structure of the RNA-dependent RNA polymerase of poliovirus, *Structure 5*, 1109−1122.
26. Gohara, D. W., Crotty, S., Arnold, J. J., Yoder, J. D., Andino, R., and Cameron C. E. (2000) Poliovirus RNA-dependent RNA polymerase (3D^{pol}): Structural, biochemical, and biological analysis of conserved structural motifs A and B, *J. Biol. Chem. 275*, 25523−25532.
27. Patel, S. S., Wong, I., and Johnson, K. A. (1991) Pre-steady-state kinetic analysis of processive DNA replication including complete characterization of an exonuclease-deficient mutant, *Biochemistry 30*, 511−525.
28. Kuchta, R. D., Mizrahi, V., Benkovic, P. A., Johnson, K. A., and Benkovic, S. J. (1987) Kinetic mechanism of DNA polymerase I (Klenow), *Biochemistry 26*, 8410−8417.
29. Reardon, J. E. (1992) Human immunodeficiency virus reverse transcriptase: Steady-state and pre-steady-state kinetics of nucleotide incorporation, *Biochemistry 31*, 4473−4479.
30. Zinnen, S., Hsieh, J. C., and Modrich, P. (1994) Misincorporation and mispaired primer extension by human immunodeficiency virus reverse transcriptase, *J. Biol. Chem. 269*, 24195−202.
31. Hsieh, J. C., Zinnen, S., and Modrich, P. (1993) Kinetic mechanism of the DNA-dependent DNA polymerase activity of human immunodeficiency virus reverse transcriptase, *J. Biol. Chem. 268*, 24607−24613.
32. Herschlag, D., Piccirilli, J. A., and Cech, T. A. (1991) Ribozyme-catalyzed and nonenzymatic reactions of phosphate diesters: rate effects upon substitution of sulfur for a nonbridging phosphoryl oxygen atom, *Biochemistry 30*, 4844−4854.
33. Arnold, J. J., Gohara, D. W., and Cameron, C. E. (2004) Poliovirus RNA-dependent RNA polymerase (3D^{pol}): Pre-steady-state kinetic analysis of ribonucleotide incorporation in the presence of Mn^{2+}, *Biochemistry 43*, 5138−5148.
34. Dahlberg, M. E., and Benkovic, S. J. (1991) Kinetic mechanism of DNA polymerase I (Klenow Fragment): Identification of a second conformational change and evaluation of the internal equilibrium constant, *Biochemistry 30*, 4835−4845.
35. Brandis, J. W., Edwards, S. G., and Johnson, K. A. (1996) Slow rate of phosphodiester bond formation accounts for the strong bias that Taq DNA polymerase shows against 2′, 3′-dideoxynucleotide terminators, *Biochemistry 35*, 2189−2200.
36. Guynn, R. W., Veloso, D., Lawson, J. W. R., and Veech, R. L. (1974) The concentration and control of cytoplasmic free inorganic pyrophosphate in rat liver in vivo, *Biochem. J. 140*, 369−375.
37. Traut, T. W. (1994) Physiological concentrations of purines and pyrimidines, *Mol. Cell. Biochem. 140*, 1−22.
38. Ferrin, L. J., and Mildvan, A. S. (1986) Studies of conformations and interactions of substrates and ribonucleotide templates bound to the large fragment of DNA polymerase I, *Biochemistry 25*, 5131−5145.
39. Ferrin, L. J., and Mildvan, A. S. (1985) Nuclear overhauser effect studies of the conformations and binding site environments of deoxynucleoside triphosphate substrates bound to DNA polymerse I and its large fragment. *Biochemistry 24*, 6904−6912.
40. Ollis, D. L., Brick, P., Hamlin, R., Xuong, N. G., and Steitz, T. A. (1985) Structure of large fragment of *Escherichia coli* DNA polymerase I complexed with dTMP, *Nature 313*, 762−766.
41. Doublie, S., and Ellenberger, T. (1998) The mechanism of action of T7 DNA polymerase, *Curr. Opin. Struct. Biol. 8*, 704−712.
42. Domingo, E., Escarmis, C., Sevilla, N., Moya, A., Elena, S. F., Quer, J., Novella, I. S., and Holland J. J. (1996) Basic concepts in RNA virus evolution, *FASEB J. 10*, 859−864.
43. Wong, I., Patel, S. S., and Johnson K. A. (1991) An induced-fit kinetic mechanism for DNA replication fidelity: direct measurement by single-turnover kinetics, *Biochemistry 30*, 526−537.
44. Kuchta, R. D., Benkovic, P. A., and Benkovic, S. J. (1988) Kinetic mechanism whereby DNA polymerase I (Klenow) replicates DNA with high fidelity, *Biochemistry 27*, 6716−6725.
45. D. W. Gohara and C. E. Cameron, unpublished results.
46. Bloomfield, V. A., Crothers, D. M., and Tinoco, I., Jr. (2000) *Nucleic Acids: Structure, Properties, and Function*, University Sciences Books, Sausilito, CA.
47. Maag, D., Castro, C., Hong, Z., and Cameron, C. E. (2001) Hepatitis C virus RNA-dependent RNA polymerase (NS5B) as a mediator of the antiviral activity of ribavirin, *J. Biol. Chem. 276*, 46094−46098.
48. Crotty, S., Maag, D., Arnold, J. J., Zhong, W., Lau, J. Y., Hong, Z., Andino, R., and Cameron, C. E. (2000) The broad-spectrum antiviral ribonucleoside ribavirin is an RNA virus mutagen, *Nat. Med. 6*, 1375−1379.
49. Streeter, D. G., Witkowski, J. T., Khare, G. P., Sidwell, R. W., Bauer, R. J., Robins, R. K., and Simon, L. N. (1973) Mechanism of action of 1-β-D-ribofuranosyl-1,2,4-triazole-3-carboxamide (Virazole), a new broad-spectrum antiviral agent, *Proc. Natl. Acad. Sci. U.S.A. 70*, 1174−1178.
50. Lin, Y. H., Yadav, P., Ravatn, R., and Stollar, V. (2000) A mutant of Sindbis virus that is resistant to Pyrazofurin encodes an altered RNA polymerase, *Virology 20*, 61−71.

BI035212Y